JOURNAL OF COMPUTATIONAL PHYSICS **140,** 1–29 (1998)
ARTICLE NO. CP975879

Nonlinear Resonance Artifacts in Molecular Dynamics Simulations*

Tamar Schlick,* Margaret Mandziuk,*,[1] Robert D. Skeel,† and K. Srinivas†

*Chemistry Department and Courant Institute of Mathematical Sciences, New York University and the Howard Hughes Medical Institute, 251 Mercer Street, New York, New York 10012; †Department of Computer Science and Beckman Institute, University of Illinois at Urbana-Champaign, 1304 West Springfield Avenue, Urbana, Illinois 61801-2987
E-mail: schlick@nyu.edu

Received August 19, 1997; revised October 21, 1997

The intriguing phenomenon of resonance, a pronounced integrator-induced corruption of a system's dynamics, is examined for simple molecular systems subject to the classical equations of motion. This source of timestep limitation is not well appreciated in general, and certainly analyses of resonance patterns have been few in connection to biomolecular dynamics. Yet resonances are present in the commonly used Verlet integrator, in symplectic implicit schemes, and also limit the scope of current multiple-timestep methods that are formulated as symplectic and reversible. The only general remedy to date has been to reduce the timestep. For this purpose, we derive method-dependent timestep thresholds (e.g., Tables 1 and 2) that serve as useful guidelines in practice for biomolecular simulations. We also devise closely related symplectic implicit schemes for which the limitation on the discretization stepsize is much less severe. Specifically, we design methods to remove third-order, or both the third- and fourth-order, resonances. These severe low-order resonances can lead to instability or very large energies. Our tests on two simple molecular problems (Morse and Lennard–Jones potentials), as well as a 22-atom molecule, N-acetylalanyl-N′-methylamide, confirm this prediction; our methods can delay resonances so that they occur only at larger timesteps (EW method) or are essentially removed (LIM2 method). Although stable for large timesteps by this approach, trajectories show large energy fluctuations, perhaps due to the coupling with other factors that induce instability in complex nonlinear systems. Thus, the methods developed here may be more useful for conformational sampling of biomolecular structures. The analysis presented here for the blocked alanine model emphasizes that one-dimensional analysis of resonances can be applied to a more complex, multimode system to analyze resonance behavior, but that resonance due to frequency coupling is more complex to pinpoint. More generally, instability, apparently due to numerically induced

[1] Present address: Chemistry Department, Long Island University, University Plaza, Brooklyn, NY 11201.

0021-9991/98 $25.00

resonances, has been observed in the application of the implicit midpoint scheme to vibrating structures and could be expected also in the simulation of nonlinear wave phenomena; in such applications it is adequate not to resolve the highest frequency modes, so the proposed methods could be very useful.

1. INTRODUCTION

The motivation for our work is development of more efficient numerical integrators for the classical-mechanics modeling of biomolecules by Newtonian physics:

$$M\frac{d^2x}{dt^2} = F(x), \tag{1}$$

where M is a diagonal matrix of masses, x is the collective position vector, t is time, and $F(x)$ is the collective force vector. Several recent reviews on algorithms for MD are available [7, 13, 21]. Many of the algorithms developed for MD apply also to other phenomena modeled by Hamiltonian systems. Such problems often involve multiple timescales spanning a wide range. As in most such problems, the highest frequencies have negligible amplitudes. Hence, the problem is "stiff-oscillatory" in the sense that there exists a much smoother trajectory of the given system (on a limited time interval) which is negligibly different from the trajectory being integrated.

Explicit integrators, such as the popular Störmer/leapfrog/Verlet method, suffer from a serious stepsize limitation due to the highest frequency components. A popular way to overcome this restriction is to impose constraints on bond lengths (and possibly bond angles) and thereby remove the highest frequencies. The effectiveness of this remedy is limited because it is based on a crude separation of high- and low-frequency modes. A constrained dynamics formulation leads to nonlinear systems of equations having nonsymmetric Jacobian matrices.

Implicit methods, on the other hand, are better than constrained dynamics for discriminating between high- and low-frequency modes. Implicit numerical integrators have been applied to problems of mechanical structures [23] and macromolecules [17, 28]. These formulations lead to symmetric matrices, which are at least twice as cheap to compute than the nonsymmetric analogs. However, these matrices are dense and typically expensive to work with. This integration subproblem of solving a nonlinear system is ameliorated by the existence of efficient solvers, like TNPACK [22], based on a minimization formulation employing preconditioned conjugate gradient and sparse matrix techniques, but implicit methods are still not generally computationally competitive with explicit formulations. Still, implicit methods might be useful for exploring phase space, that is, finding conformations of low free energy and suggesting pathways for conformational changes [11, 6]. Current techniques for enhanced sampling, like high-temperature dynamics, misrepresent the true dynamics. In addition, cheap imitations of implicit methods, which are implicit in only the stiffest terms and/or are only linearly implicit [30], might be useful.

Symplectic integrators form a large class of methods that possess favorable properties for the numerical simulation of Hamiltonian dynamical systems [19]. In particular, symplecticness in the small-timestep regime implies numerical stability without artificial

damping. However, when multiple timescales are present in the physical system, this numerical stability can typically be attained only if the timestep size is limited to less than the value based on accuracy considerations alone.

To circumvent this timestep limitation, *implicit* symplectic schemes have been applied. Unfortunately, at large timesteps relative to the period of the fastest motion in the system, even implicit symplectic integrators can become unstable when applied to nonlinear Hamiltonian systems. This type of instability has been reported for the implicit midpoint (IM) method [9, 13, 24] and is surprising, given that IM is not only unconditionally stable for a harmonic oscillator but exactly conserves energy for all time-steps, Δt.

In a more recent study of a nonlinear oscillator integrated by IM, Mandziuk and Schlick [15] offered additional insights into the mechanisms that trigger nonlinear instability. They related the numerically perturbed period of the oscillator to the timestep of discretization and observed high energetic fluctuations, or instability, when these two are in resonance. This purely numerical artifact is especially severe for third- and fourth-order resonance and, in the case of the former, always leads to instability. (The resonance order n refers to the number of phase space points sampled in a closed orbit of a finite period. A resonance is labeled $m:n$ if a period cycle of length n involves m rotational sweeps in phase space.) Furthermore, for the Verlet scheme, it was shown [15] that instability occurs at timesteps which satisfy the linear stability condition. These instabilities can only be avoided by restricting Δt.

Hints of resonance problems can also be found in an interesting article of Sanz-Serna [20]. This study applied the Moser twist theorem to show that if third (3:1) and fourth (4:1) order resonances can be avoided, stability at equilibrium is guaranteed for the symplectic Euler method (equivalent to the leapfrog/Verlet method). The consequences of these resonances are not discussed; see also Ref. [16]. Nonlinear resonance has also been observed in an explicit semi-analytical symplectic integrator for planetary motion [27].

In general, nonlinear instabilities are encountered for substantially smaller stepsizes than those predicted by linear stability analysis. Uncovering their primary source in macromolecular dynamics with large timesteps is important for overcoming the instability problem and increasing the feasible timestep of integration. Finding cures besides just reducing the timestep forms a major challenge.

In this paper, we present a family of symplectic schemes closely related to IM [25] for which there is no such stability limitation on the timestep. To illustrate this idea and analyze nonlinear resonances, we apply IM, Verlet, and two new symplectic schemes (EW and LIM2) to two simple nonlinear systems: two atoms interacting via Morse or Lennard-Jones potential. To test the idea on a multimode system, we also apply the integrators to a 22-atom molecule, N-acetylalanyl-N′-methylamide (commonly known as alanine dipeptide), modeled with the CHARMM forcefield [5]. We thus show how methods can be designed to delay or essentially eliminate resonance per se and also how simple one-dimensional analysis of resonances is useful for analyzing behavior in a more complex molecular system.

In the next section, we review the integration methods used in this paper. Section 3 discusses the resonance conditions for these schemes and presents methodologies for removal of instabilities. In Section 4, the results of simple numerical experiments are presented, and in Section 5 the results for alanine dipeptide are reported. Conclusions are summarized in Section 6.

2. A ONE-PARAMETER FAMILY OF INTEGRATION METHODS

A. *Definitions*

When IM is applied to a harmonic oscillator, the oscillation frequency is distorted depending on Δt. As a result, the numerical phase-angle change per timestep suffers a reduction from its actual value. This reduction becomes dramatic as the timestep increases. The phase-angle change never exceeds π radians per timestep, regardless of the analytical value.

To clarify the relation among various methods, we formulated a one-parameter family of symplectic integrators [25]. The family's unifying feature is the discrete approximation to the force vector F at time $n\Delta t$:

$$F^n = F(X^n + \alpha \Delta t^2 M^{-1} F^n). \tag{2}$$

Here, X^n represents the discrete approximation to x at time $n\Delta t$, and the parameter α characterizes each method in the family. The value $\alpha = \frac{1}{4}$ corresponds to IM (which is equivalent to the trapezoid method); $\alpha = \frac{1}{12}$ becomes the fourth-order Störmer–Cowell/Numerov method, and $\alpha = 0$ is the known Verlet scheme [25]. The integration scheme is implicit when $\alpha > 0$.

The parameter α affects the relationship between the numerical frequency and the actual frequency of the system. Specifically, the maximum possible phase angle change per timestep *decreases* as the parameter α *increases*. Hence, the angle change can be limited! In particular, the choice $\alpha \geq \frac{1}{2}$ limits the phase angle change to less than one-quarter of a period. This should ensure that notable oscillations will not occur due to fourth-order resonance. The scheme corresponding to $\alpha = \frac{1}{2}$ was suggested by Zhang and Schlick [29], where it was termed LIM2 (for a midpoint-variation scheme designed for Langevin dynamics). The choice $\alpha \geq \frac{1}{3}$ (including LIM2) guarantees that the phase angle change per timestep is less than one-third of a period and avoids nonlinear instability for the Morse potential. We call the scheme corresponding to $\alpha = \frac{1}{3}$ "equally weighted" (EW), since the discrete position vectors at three consecutive timesteps, X^{n-1}, X^n, X^{n+1}, are equally weighted for the force evaluation in a particular form [25] of the scheme (which we call 2M).

The family of methods characterized by Eq. (2) has several equivalent discretization forms [25] for a given α. This equivalence means that a local transformation exists to relate the state variables of one method at a given time to those of the other method.

In this article we use the family form "OneM" (to designate a one-step method and a midpoint evaluation of forces) [25]. Assuming that at time $n\Delta t$ the position and velocity vectors X^n and V^n are known, the propagation to time $(n+1)\Delta t$ is then defined by the expressions:

$$X^{n+1/2} = X^n + \frac{\Delta t}{2} V^n, \tag{3a}$$

$$F^{n+1/2} = F(X^{n+1/2} + \alpha \Delta t^2 M^{-1} F^{n+1/2}), \tag{3b}$$

$$V^{n+1} = V^n + \Delta t M^{-1} F^{n+1/2}, \tag{3c}$$

$$X^{n+1} = X^{n+1/2} + \frac{\Delta t}{2} V^{n+1}. \tag{3d}$$

The equation for $F^{n+1/2}$ is implicit for $\alpha \neq 0$ (i.e., the unknown force vector appears at both sides of the equation and cannot be obtained in closed form). Assuming that system

(1) is conservative, with $F(x) = -\nabla U(x)$, the negative gradient of the potential energy, system (3) can be solved by minimizing the *dynamics function*

$$\Phi(X) = \frac{1}{2}\Delta t^{-2}\left(X - X_0^n\right)^{\mathrm{T}} M\left(X - X_0^n\right) + \alpha U(X) \tag{4}$$

for X and then evaluating F at this point. Here $X_0^n = X^n + (\Delta t/2)V^n$; see Refs. [17, 29] for derivation of the dynamics function for implicit methods.

B. *Linear Stability and Energy Conservation*

We now discretize the equations governing the motion of a harmonic oscillator by system (3) and perform algebraic rearrangements to obtain the recurrence expressions

$$\begin{bmatrix} \omega X^{n+1} \\ V^{n+1} \end{bmatrix} = S \begin{bmatrix} \omega X^n \\ V^n \end{bmatrix} \tag{5}$$

for the positions and velocities, where the matrix

$$S = \begin{bmatrix} 1 - \frac{1}{2}(\omega\Delta t)^2\phi & \omega\Delta t\left(1 - \frac{1}{4}(\omega\Delta t)^2\phi\right) \\ -\phi\omega\Delta t & 1 - \frac{1}{2}(\omega\Delta t)^2\phi \end{bmatrix} \tag{6}$$

and the parameter

$$\phi = (1 + (\omega\Delta t)^2\alpha)^{-1}. \tag{7}$$

Thus, the evolution of the discrete system depends on the properties of the matrix S. Linear stability is achieved when $(\omega\Delta t)^2\phi < 4$, i.e.,

$$(\omega\Delta t)^2/(1 + (\omega\Delta t)^2\alpha) < 4. \tag{8}$$

In this case, S has imaginary eigenvalues, $\exp(\pm i\omega_{\mathrm{eff}}\Delta t)$, where

$$\begin{aligned} \omega_{\mathrm{eff}}\Delta t &= 2\arcsin\left(\frac{\omega\Delta t}{2}\sqrt{\phi}\right) \\ &= \omega\Delta t + \left(\frac{1}{24} - \frac{\alpha}{2}\right)(\omega\Delta t)^3 + O((\omega\Delta t)^5). \end{aligned} \tag{9}$$

Consequently, S can be decomposed as

$$S = DQD^{-1}, \tag{10}$$

where

$$Q = \begin{bmatrix} \cos\omega_{\mathrm{eff}}\Delta t & \sin\omega_{\mathrm{eff}}\Delta t \\ -\sin\omega_{\mathrm{eff}}\Delta t & \cos\omega_{\mathrm{eff}}\Delta t \end{bmatrix} \tag{11}$$

and

$$D = \mathrm{diag}\left[1, \left(1 + \left(\alpha - \frac{1}{4}\right)(\omega\Delta t)^2\right)^{-1/2}\right]. \tag{12}$$

The matrix Q represents a rotation of $-\omega_{\mathrm{eff}}\Delta t$ radians in phase space.

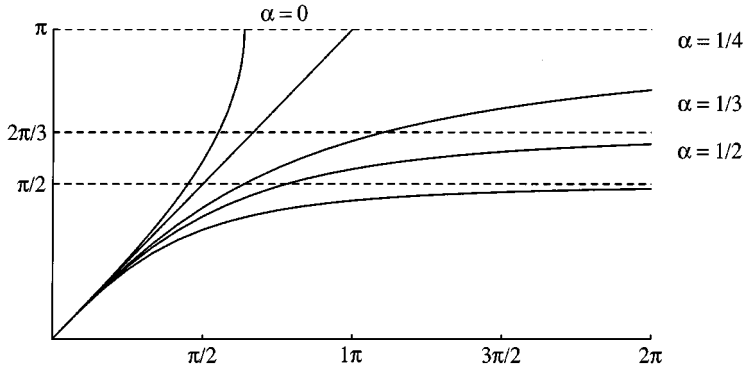

FIG. 1. Effective rotation ($\omega_{\text{eff}}\Delta t$) from Eq. (9) versus desired rotation ($\omega\Delta t$) for one timestep for $\alpha = 0, \frac{1}{4}, \frac{1}{3}, \frac{1}{2}$.

Note that $\alpha = \frac{1}{4}$ (IM method) implies that D is the identity matrix, rendering the transformation unitary and guaranteeing exact energy conservation [25]. For other values of α, the energy oscillates; the ratio of the maximum to minimum energy is given by $\max\{1 + (\alpha - \frac{1}{4})(\omega\Delta t)^2, (1 + (\alpha - \frac{1}{4})(\omega\Delta t)^2)^{-1}\}$. Furthermore, deviations of D from the identity matrix adversely affect the time-averaged partitioning of energy between kinetic and potential energy.

Figure 1 shows the effective rotation versus the desired rotation for $\alpha = 0, \frac{1}{4}, \frac{1}{3}, \frac{1}{2}$ according to Eq. (9). (For IM, Eq. (9) simplifies to $\omega_{\text{eff}}\Delta t = 2\arctan(\omega\Delta t/2)$). The straight line represents the ideal value. We see that, when $\omega\Delta t$ is small, all curves approximate the straight line well, but as $\omega\Delta t$ increases the curves exhibit different behavior. As $\omega\Delta t \to +\infty$, the effective rotations for $\alpha = \frac{1}{4}, \frac{1}{3}, \frac{1}{2}$ approach the limiting values of $\pi, 2\pi/3, \pi/2$, respectively.

C. *Postprocessing*

Interestingly, the symplectic transformation

$$x^n = \left(1 + \left(\alpha - \frac{1}{4}\right)(\omega\Delta t)^2\right)^{-1/4} X^n, \quad p^n = \left(1 + \left(\alpha - \frac{1}{4}\right)(\omega\Delta t)^2\right)^{1/4} P^n \tag{13}$$

yields "postprocessed" values that exactly conserve energy [25]. (Here we use momenta P and p instead of velocity V.) It is unclear, however, how to define a meaningful transformation for postprocessing the values obtained for the general nonlinear conservative system (Eq. (1)) so that energy conservation is achieved if the system is linear. For this purpose, we propose the transformation

$$x = X + \psi(\eta M^{-1}U_{xx}(X))\eta M^{-1}U_x(X), \tag{14}$$

$$p = \left(I + (\psi(\eta M^{-1}U_{xx}(X))\eta M^{-1}U_x(X))_X\right)^{-\mathrm{T}} P, \tag{15}$$

where the subscript X denotes differentiation with respect to X, $\eta = (\alpha - \frac{1}{4})(\Delta t)^2$, and

$$\psi(\xi) = \frac{(1+\xi)^{-1/4} - 1}{\xi} = -(1+\xi)^{-1/4}(1 + (1+\xi)^{1/4})^{-1}(1 + (1+\xi)^{1/2})^{-1}. \tag{16}$$

This function is well defined if ξ is generalized to a symmetric positive definite matrix.

The postprocessing formulation above is symplectic for general nonlinear problems and yields values x and p that exactly conserve energy in the linear case. (To see that the transformation is symplectic, note that it arises from the second-kind generating function $S(X, p) = p^{\mathrm{T}}X + p^{\mathrm{T}}\psi(\eta M^{-1}U_{xx}(X))\eta M^{-1}U_x(X))$. This transformation is not cheap, but it is not intended to be applied in practice. Rather, its purpose here is to permit comparison of methods on the basis of the accumulating part of the error, not removable by a phase space transformation. For a cheaper postprocessing, we could approximate ψ by a polynomial on some interval of values with ξ ranging from 0 to $(\alpha - \frac{1}{4})(\omega\Delta t)^2$. Further approximations are also possible [14, 25] based on differencing the computed values of X and P.

The transformation (14), (15) is not necessarily the one that best conserves the energy; rather it is a heuristic choice that does remarkably well. Postprocessing is discussed further in Refs. [14, 25], where it is shown that there are limits on the accuracy improvements that are possible with such transformations.

3. NONLINEAR INSTABILITY, RESONANCE, AND A POSSIBLE CURE

Nonlinear stability for fixed Δt can be investigated analytically in the neighborhood of an energy minimum (x_0, p_0) for a system with one degree of freedom via the Moser twist theorem. Analysis is possible via asymptotic expansions in powers of $x - x_0$ and $p - p_0$. Essentially behavior depends on the angle of rotation per step (see Appendix 7 of Ref. [1]); and is given by the linear terms of the expansion. If this is one-third of a circle (3 : 1 resonance), the equilibrium point is unstable. If it is one-fourth of a circle (4 : 1 resonance), the situation is indeterminate—it will depend on the mapping defined by one timestep of the method applied to the problem. For higher order resonances (e.g., rotation of two-fifths of a period, 5 : 2 resonance), the equilibrium point is normally stable [20]. The result in [20] can be paraphrased as follows: Assume that we have a numerical method described by an area-preserving map in the plane for which the origin is an elliptic equilibrium so that the eigenvalues of the linearized map are complex conjugates λ and $\bar{\lambda}$ with unit modulus. Further, assume that λ is neither a cubic nor a fourth root of unity. Then the origin is a stable equilibrium except, perhaps, in the "degenerate" case that the mapping acts as a rigid rotation plus terms of order 4 in $x - x_0$ and $p - p_0$.

Mandziuk and Schlick observed that IM applied to the Morse oscillator (see formulation below) exhibits instability for the 3 : 1 resonance but not for 4 : 1 nor higher-order resonances (although energy fluctuations are very large) [15]. For a large complex system with many fundamental frequencies or instantaneous normal modes, this suggests that the timestep must *be limited to less than one-third or one-quarter of the effective period of the highest-frequency mode*, depending on the scheme and possibly the problem.

It is evident from Eq. (9) and Fig. 1 that a sufficiently large α can lower the maximum rotation angle per step as needed. In particular, since a resonance of order n means that n phase space points are computed per effective period, resonances of order n and lower will be eliminated if α is large enough so that the numerical rotation per step satisfies

$$\omega_{\mathrm{eff}}\Delta t < 2\pi/n \tag{17}$$

for all Δt. This is equivalent to

$$\alpha \geq \left(2\sin\frac{\pi}{n}\right)^{-2}. \tag{18}$$

The first few values given by this formula are

n	2	3	4	5	6
α	$\frac{1}{4}$	$\frac{1}{3}$	$\frac{1}{2}$	$\frac{(5+\sqrt{5})}{12}$	1

The value $\alpha = \frac{1}{4}$ (IM scheme) is the minimum value needed for unconditional linear stability; the value $\alpha = \frac{1}{3}$ (EW scheme) is the smallest value that guarantees unconditional nonlinear stability for the Morse potential; and the value $\alpha = \frac{1}{2}$ (LIM2) or greater guarantees nonlinear stability for general potentials.

For a given α, we can also calculate the *upper limit* on the *timestep* (rather than lower limit on α) needed to avoid a resonance of order n. Specifically, if $(2\sin(\pi/n))^{-2} > \alpha$, a timestep satisfying

$$\omega\Delta t < \frac{2\sin(\pi/n)}{\sqrt{1-4\alpha\sin^2(\pi/n)}} \tag{19}$$

avoids a resonance of order n.

In Table 1 we list these limiting values for interesting combinations of α and n. The values for $n=2$ are also the limits on $\omega\Delta t$ for linear stability. We show in the next section for Morse and Lennard–Jones potentials that for Verlet ($\alpha = 0$) the 4 : 1 resonance is unstable, and hence nonlinear stability imposes a restriction of $\sqrt{2}$ on $\omega\Delta t$, significantly less than the linear limit of 2. Experiments suggest, however, that the 4 : 1 resonance is stable for $\alpha = \frac{1}{4}, \frac{1}{3}, \frac{1}{2}$. This points to a nonlinear stability limit of $2\sqrt{3}$ for IM ($\alpha = \frac{1}{4}$) and no restriction for EW ($\alpha = \frac{1}{3}$). Numerical results also suggest significant fluctuations due to 5 : 1 and 6 : 1 resonances for Verlet, 4 : 1 and 5 : 1 resonances for IM, and 4 : 1 resonance for EW. In contrast, LIM2 ($\alpha = \frac{1}{2}$) exhibits no such erratic patterns.

In unconstrained molecular dynamics of biomolecules modeled at atomic resolution, the highest mode has a period of about 9 fs, corresponding to a vibrational frequency of 3600 cm^{-1}. For Verlet, the analysis above suggests a limit on the timestep of 2.0 fs to prevent instability, 1.7 fs to avoid 5 : 1 resonances, and 1.4 fs to avoid 6 : 1 resonances.

Not surprisingly, we face a trade-off between stability and accuracy. As indicated by Eq. (9), the discretization error is proportional to $|\alpha - \frac{1}{12}|$ for small $\omega\Delta t$, so IM has twice the error of Verlet, EW has three times the error of Verlet, and LIM2 has an error larger by a factor of five. This is not the case, though, for large values of $\omega\Delta t$ (Fig. 1), for which the Verlet curve diverges most rapidly. In addition, when stability is limiting the stepsize, EW (and possibly also LIM2) permits a larger timestep than does Verlet for equal accuracy.

TABLE 1
Stability Limit on $\omega\Delta t$ for Interesting Combinations of α and n

Resonance order	Verlet ($\alpha = 0$)	IM ($\alpha = \frac{1}{4}$)	EW ($\alpha = \frac{1}{3}$)
$n = 2$	2	∞	∞
$n = 3$	$\sqrt{3} \approx 1.72$	$2\sqrt{3} \approx 3.46$	∞
$n = 4$	$\sqrt{2} \approx 1.41$	2	$\sqrt{6} \approx 2.45$
$n = 5$	$\frac{1}{2}\sqrt{10-2\sqrt{5}} \approx 1.18$	$2\sqrt{5-2\sqrt{5}} \approx 1.45$	
$n = 6$	1		

4. SIMPLE NUMERICAL EXPERIMENTS: EW, LIM2 AND IM VERSUS VERLET

We first examine simple systems where resonance phenomena are much easier to observe and interpret.

A. *Morse Potential*

We begin with the HBr Morse potential as used previously [15],

$$U(r) = D\left(1 - e^{-S(r-r_0)}\right)^2, \tag{20}$$

where r is the bond length, $D = 90.5$ kcal/mol, $S = 1.814$ Å^{-1}, and $r_0 = 1.41$ Å (1 kcal mol $= 4.184 \times 10^{-4}$ amu Å^2/fs^2). The two atoms with masses m_1 and m_2 move in one dimension. Their positions are denoted as x_1 and x_2 ($x_1 < x_2$), and they interact according to the force produced by the potential $U(r)$. The bond length is then given by $r = x_2 - x_1$, and its conjugate momentum by $p = \mu(\dot{x}_2 - \dot{x}_1)$, where μ is the reduced mass of the diatom: $\mu = m_1 m_2/(m_1 + m_2)$. In terms of these variables, the motion of the system satisfies the equations

$$\dot{r} = \frac{p}{\mu}, \quad \dot{p} = -U_r(r), \tag{21}$$

associated with the Hamiltonian

$$\frac{p^2}{2\mu} + U(r) + \text{constant translational kinetic energy}. \tag{22}$$

As before, we use $m_1 = 1.00785$ amu and $m_2 = 79.904$ amu for the hydrogen and bromine atoms, respectively ($\mu = 0.9953$ amu) [15]. For the calculations illustrated in Figs. 2 and 3 the same initial conditions are also used: $r(0) = 1.4155$ Å and $p(0) = \mu(1.545$ Å$)/(48.888$ fs).

To inspect resonance trends, we compute the energy variation as a function of Δt. The reported values represent the *maximum energy variation* over 1000 steps, *expressed relative to the initial energy*. The interval between various timesteps is chosen adaptively, so as to achieve an informative plot clustering near resonances.

The effect of reducing the energy error by postprocessing for Verlet and EW can be seen in Fig. 2 (recall that postprocessing has no effect for IM). Plotted for a range of timesteps is the relative energy variation for a solution not subject to postprocessing, a cheaply postprocessed solution that uses central time differencing [25], and a fully postprocessed solution.

For Verlet (Fig. 2a), the graphs have spikes of increasing heights corresponding to 7 : 1, 6 : 1, 5 : 1, and 4 : 1 resonances, the last of which becomes unstable. The straight dashed line corresponds to the depth of the potential energy well. This plot is very similar to that shown in Mandziuk and Schlick [15]. It is different, however, from Fig. 4 of Ref. [16], where the maximum energy variation is plotted as a function of initial energy for a fixed timestep; this latter plot is based on the same data as numerical phase space plots, which we give in Figs. 5b–5d. For EW, in contrast to Verlet, only the 4 : 1 resonance appears (for all three degrees of postprocessing) and it is stable (Fig. 2b). Note, that the timestep range for EW is five times larger than for Verlet. Also observe that resonance fluctuations in both figures are revealed more clearly after postprocessing. For that reason, in the further analysis in this section, only postprocessed results are displayed.

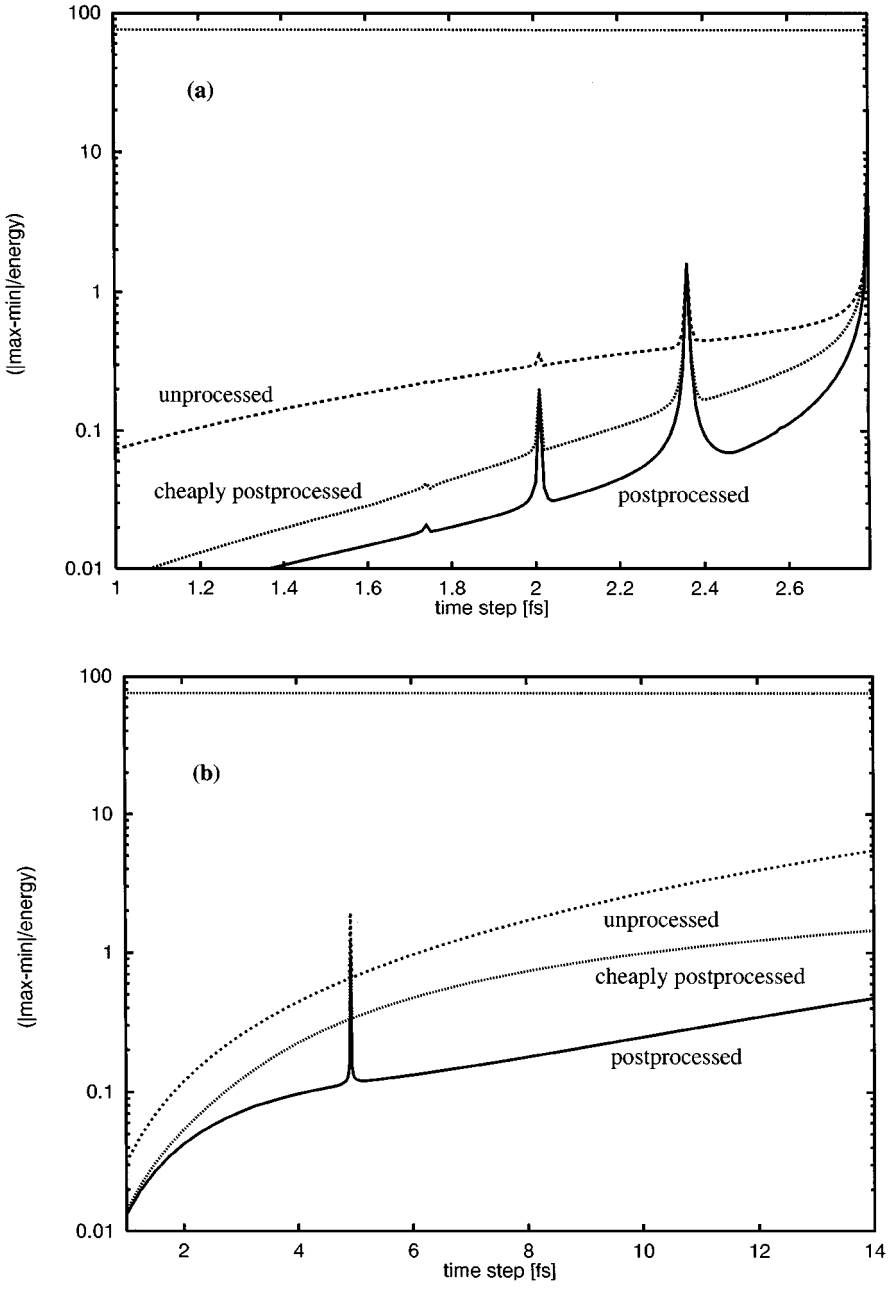

FIG. 2. The effect of postprocessing on relative energy variation versus timestep for the Morse oscillator for the (a) Verlet ($\alpha = 0$) and (b) EW ($\alpha = \frac{1}{3}$) schemes. Shown for comparison is the dissociation energy D divided by the initial energy.

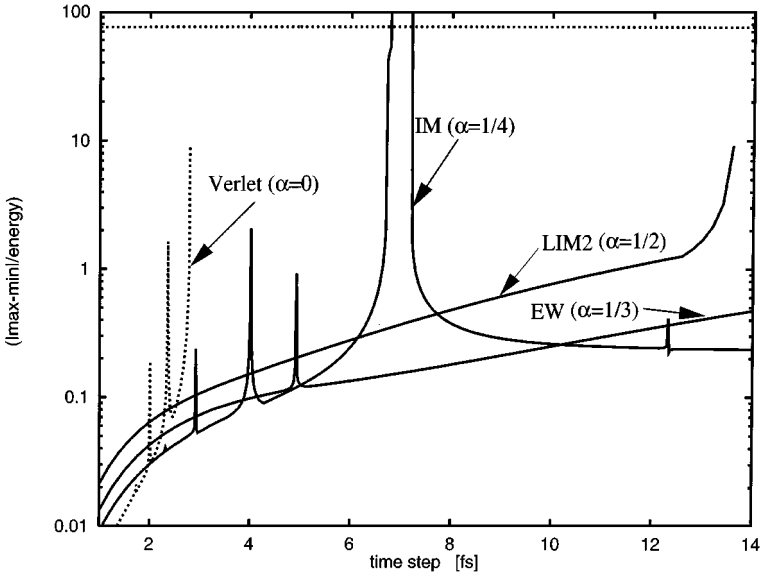

FIG. 3. Relative energy variation versus timestep for the Morse oscillator for postprocessed Verlet ($\alpha = 0$, dashed line) and IM ($\alpha = \frac{1}{4}$, solid line with instability near 7 fs), postprocessed EW ($\alpha = \frac{1}{3}$, thick solid line with only one peak near 5 fs), and postprocessed LIM2 ($\alpha = \frac{1}{2}$, solid line with no peaks). Shown also is the dissociation energy D divided by the initial energy.

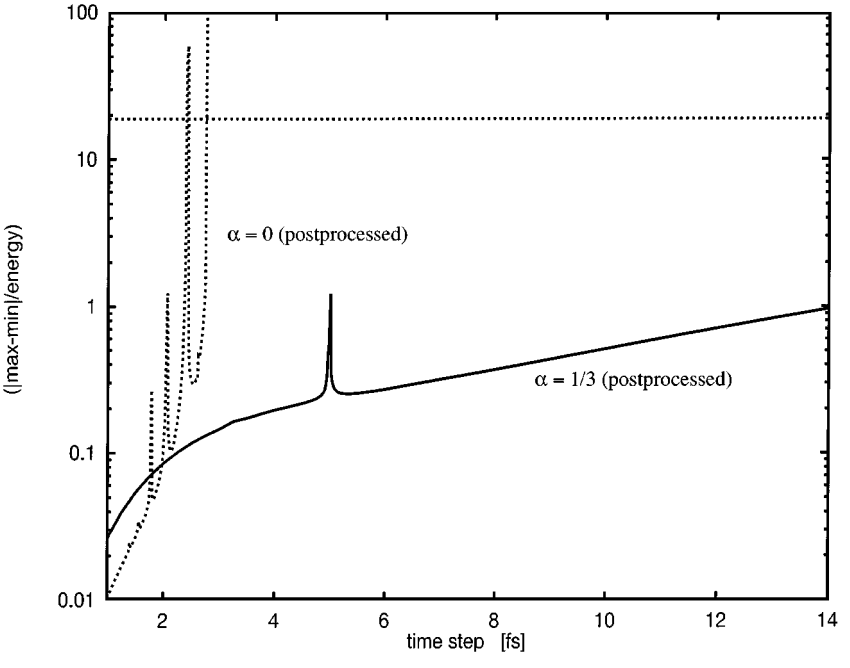

FIG. 4. Relative energy variation versus timestep for *higher initial energy* for postprocessed Verlet ($\alpha = 0$, dashed line) and postprocessed EW ($\alpha = \frac{1}{3}$, solid line). Shown also is the dissociation energy D divided by the initial energy.

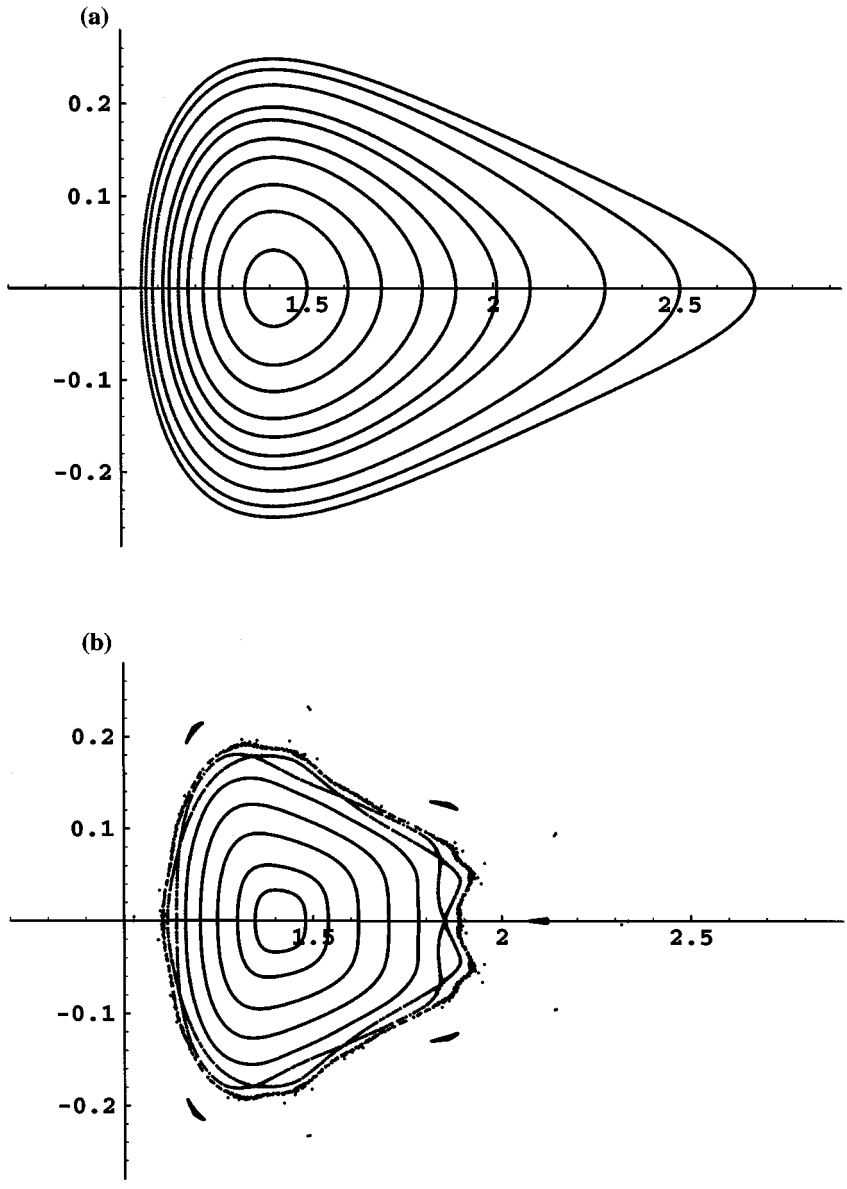

FIG. 5. Morse oscillator orbits for increasing values of energy: (a) analytical solutions, versus numerical solutions at $\Delta t = 4$ fs: (b) IM ($\alpha = \frac{1}{4}$); (c) EW ($\alpha = \frac{1}{3}$); and (d) LIM2 ($\alpha = \frac{1}{2}$).

The relative energy variations for the three implicit methods (IM, EW, LIM2) are presented in Fig. 3 and compared to results obtained with Verlet. The graph for IM (bottom solid line) has, from left to right: spikes of increasing heights, corresponding to the 6 : 1, 5 : 1, and 4 : 1 resonances; an open peak around $\Delta t = 7$ fs for the unstable 3 : 1 resonance; and a spike around 12 fs for the 5 : 2 resonance. (The n : m resonance can be identified from the trajectory values as a periodic cycle of length n involving m rotational sweeps in phase space). For EW (middle solid line), the 4 : 1 resonance is significantly less severe than the 5 : 1 resonance of Verlet. LIM2 (top solid line), which corresponds to the largest α, does

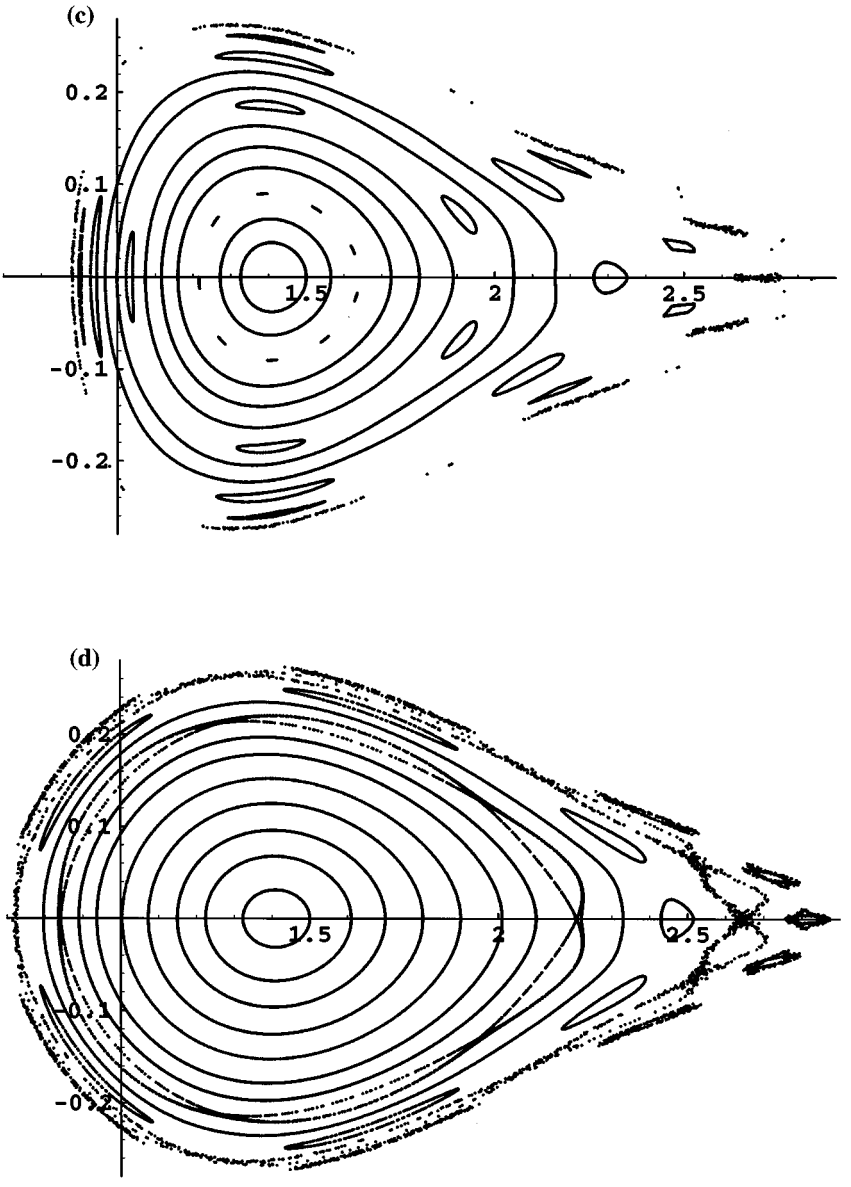

FIG. 5—*Continued*

not exhibit resonance, but rather a difficulty in solving the nonlinear equation for large timesteps. The energy error is also larger.

Figure 4 shows the effect of increasing the initial energy for EW and Verlet; by doubling both $p(0)$ and $r(0) - r_0$, we roughly quadruple the energy error. Now we see an increase in the error, but the resonance pattern remains essentially the same (compare with Fig. 3).

Nonlinear resonances can also be visualized from phase-space portraits as island regions. In Fig. 5a we show the analytical orbits for the Morse oscillator corresponding to increasing energy levels (from the innermost orbit outward) [15]. Figures 5b–5d show the phase space portraits corresponding to IM, EW, and LIM2, respectively, each with $\Delta t = 4$ fs. The period

of the Morse oscillator is energy dependent and for the range for energies covered in Fig. 5a it varies from around 12.5 fs to 40 fs. The plot for IM reveals resonances of orders 9 : 2, 5 : 1, and 6 : 1. The 9 : 2 resonance is just outside the inner two orbits (it was determined to be 9 : 2 rather than 9 : 1 resonance by inspection of the trajectory). The 5 : 1 and 6 : 1 resonances are outside, in a chaotic sea of instability. EW (Fig. 5c) exhibits resonances of orders 9 : 2, 5 : 1, 6 : 1, 7 : 1, and 8 : 1. LIM2 shows resonances of orders 6 : 1, 7 : 1, 8 : 1, and 9 : 1.

It is clear from the plots that with increasing α the onset of chaos is shifted towards higher energies (lower frequencies). In all cases, however, there are serious deviations from the analytic trajectory as the energy increases. The square-shaped, lower energy contours for IM indicate the timestep proximity to the fourth-order resonance. The contours for EW and LIM2 are smoother, but with increasing α the region of phase space with a bond length below the equilibrium value is more corrupted.

B. *Lennard–Jones Potential*

We now consider a Lennard–Jones potential describing the interaction between two argon atoms [18],

$$U(r) = \epsilon(1 - 2(\sigma/r)^6)^2, \tag{23}$$

where $\epsilon = 120\ \mathrm{K} \times k_\mathrm{B}$ and $\sigma = 3.4$ Å (the Boltzman constant $k_\mathrm{B} = 8.244 \times 10^{-7}$ amu Å^2/fs^2/K). We use the masses $m_1 = m_2 = 39.95$ amu ($\mu = 19.975$ amu) and the initial conditions $r(0) = 1.15\sigma$ and $p(0) = 0$.

Figure 6 shows the corresponding energy for Verlet, IM, and EW. The dotted curve, for Verlet, has from left to right spikes of increasing height for the 7 : 1, 6 : 1, and 5 : 1 resonances. The solid graph, for IM, has a spike for the 6 : 1 resonance. The dashed curve for EW has no spikes. Verlet is more accurate than IM and EW at small timesteps. That trend reverses with increased Δt. It appears that overall energy fluctuations, as well as nonlinear

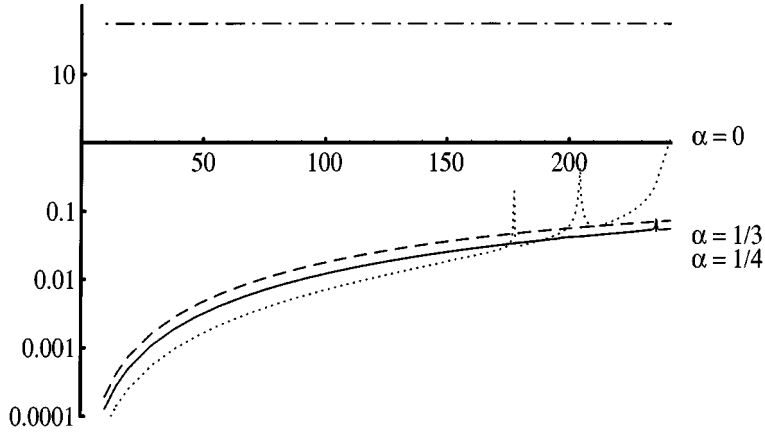

FIG. 6. Relative energy variation for postprocessed Verlet ($\alpha = 0$, dotted line) versus IM ($\alpha = \frac{1}{4}$, solid line) and EW ($\alpha = \frac{1}{3}$, dashed line), obtained for a Lennard–Jones potential for argon as a function of the timestep. Shown also is the dissociation energy ϵ divided by the initial energy.

resonance peaks, are far less dramatic for the Lennard–Jones than the Morse potential. Typically, only the Lennard-Jones potential is used in most biomolecular force fields.

In sum, simulation results for these simple systems clearly show that our symplectic implicit schemes EW ($\alpha = \frac{1}{3}$) and LIM2 ($\alpha = \frac{1}{4}$) eliminate the low-order resonances that lead to the highest energy fluctuations or instability in other methods like IM. Our postprocessing strategy is effective for accentuating resonance trends. Still, energy fluctuations are relatively large even without the sharp resonance effect, and these effects on the system's dynamic properties should be more closely examined.

5. APPLICATION TO MOLECULAR DYNAMICS OF A PEPTIDE MODEL

Our goals in this section are twofold. First, we seek to determine whether the symplectic implicit integrators EW and LIM2 improve numerical behavior over IM by eliminating, or reducing the severity of, low-order resonances. Second, we seek to establish how good our harmonic-oscillator analysis of resonances for IM is for a complex, nonlinear, and multiple-timescale system. In particular, is it possible to determine the discrete timestep values, where a resonance of a given order will occur? That is, can the source of resonance be attributed to one vibrational mode? Furthermore, if discrepancies occur between linear theory and nonlinear applications, how large are they and how can they be interpreted?

We choose the model system N-acetylalanyl-N′-methylamide shown in Fig. 7. Its chemical composition is given by CH_3–CO–NH–$CHCH_3$–CO–NH–CH_3. This 22-atom system contains representative characteristics of polypeptides (such as main chain dihedral-angle motion) and is particularly flexible, making it a good test case.

Calculations were performed with the CHARMM program [5] (version 24b1), modified to perform implicit integration in the OneM form (system (3)) for a specified $\alpha > 0$. An all-atom representation was used with the CHARMM parameter set 22. Minimization of the dynamics function (4) was accomplished with the truncated-Newton minimization package TNPACK [22], using X^n as the initial condition. The TNPACK convergence parameter EPSF was set in the range 10^{-10}–10^{-12}. Even though the timestep in the implicit scheme is larger by a factor of up to 10, the implicit schemes are more expensive for covering the total trajectory time. As we have shown in a closely related context [2], speedup in reference to explicit simulations at 0.5-fs timesteps would only be obtained for the dipeptide when the timestep exceeds 20 fs.

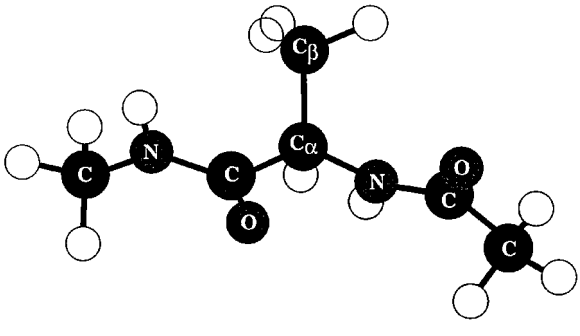

FIG. 7. Blocked alanine ("dipeptide") model.

To identify the timesteps at which instabilities occur, trajectories of 100,000 steps were analyzed for a range of timesteps (in increments of 0.1 fs). For the smallest Δt used, 1 fs, 100,000 steps correspond to 100 ps. The average values of the total energy E and its components are accumulated and displayed after 20,000, 60,000, and 100,000 steps to clarify the energetic convergence pattern. Plots of $\langle E \rangle$ versus Δt for Verlet, IM, EW, and LIM2 are shown in Fig. 8. We emphasize that longer simulations, or a more frequent sampling of Δt and different starting points, might produce different curves.

Note also that Fig. 8 reveals a quadratic growth of error with the timestep, confirming the second-order accuracy of the symplectic methods applied here. Low-order methods are typically used in biomolecular MD since the highly approximate nature of the potential functions does not merit high-order integrators. In addition, the existence of serious instabilities due to the very stiff, oscillatory high-frequency degrees of freedom argues against higher-order schemes which will likely only have stricter restrictions on the timestep, thereby increasing the practical simulation cost considerably.

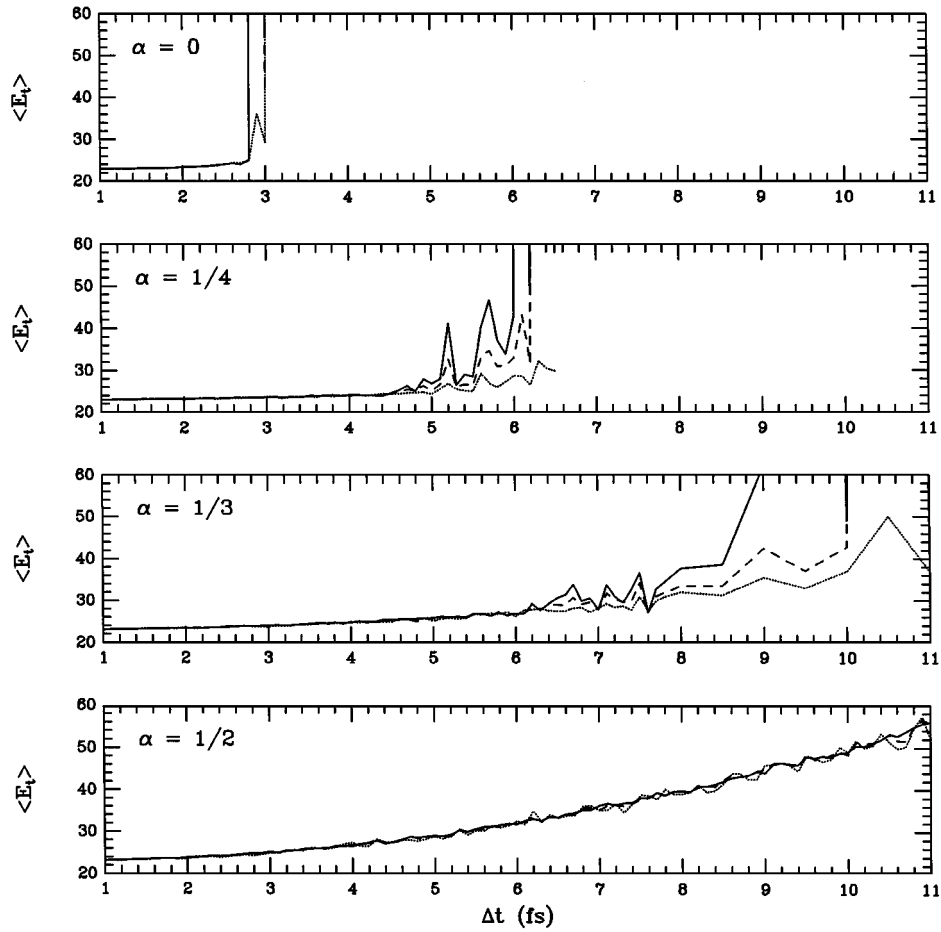

FIG. 8. E vs Δt for the Verlet ($\alpha = 0$), IM ($\alpha = \frac{1}{4}$), EW ($\alpha = \frac{1}{3}$), and LIM2 ($\alpha = \frac{1}{2}$) schemes for the peptide model. The three lines correspond to averaging energies over an increasing number of steps: 2×10^4 (dotted line); 6×10^4 (dashed line); and 10^5 (solid line).

A. *The Effect of the Parameter α*

Instabilities are revealed in Fig. 8, which displays patterns of $\langle E \rangle$ versus Δt for the Verlet, IM, and EW schemes. As expected from our analysis of simple problems, the onset of instability is delayed with increasing α. For Verlet, the onset of instability emerges at timesteps around 2.8 fs. For IM, instability emerges around 4.5 fs, and for EW around 6 fs. The plot for LIM2 (bottom panel) does not display energy spikes. Instead, $\langle E \rangle$ increases smoothly, but significantly, over the range of analyzed Δt (1–11 fs).

B. *Resonance Analysis of IM*

Explaining the instabilities is much more involved for a multimode system than for a simple system. First, an accurate comparison of fluctuations would require a more extended sampling of their values than done here. This entails very long calculations for each timestep—especially near resonances. (For the Morse oscillator we used 100,000 steps to ensure reasonable convergence near resonance [15].) Second, intramolecular energy transfer prevents clear analysis of the resonance origin; it cannot be easily determined whether certain modes are more active due to numerical artifacts or to mode coupling. In addition, the interplay between these two factors makes the long calculations impractical for resonance diagnostics—extension of simulation time increases the probability of energy transfer.

To identify the fastest modes in alanine dipeptide and apply our analysis for one-dimensional (1D) systems [15], we generated a power spectrum (Fig. 9) from an IM trajectory using $\Delta t = 0.5$ fs. The main peaks in the high frequency region correspond to N–H bond stretching around 0.63 fs^{-1} (period of 9.97 fs) and C–H bond stretching around 0.55 fs^{-1} (period of 11.42 fs). In Table 2 we list the timesteps for IM and Verlet that lead to 3 : 1 and 4 : 1 resonances for these frequencies according to our 1D analysis. A comparison of the values in Table 2 with Fig. 8 reveals the possible cause of instability.

For Verlet, instability may result from the third-order resonance of an N–H stretch, the fourth-order resonance of a C–H stretch, or an interplay between both vibrations. However,

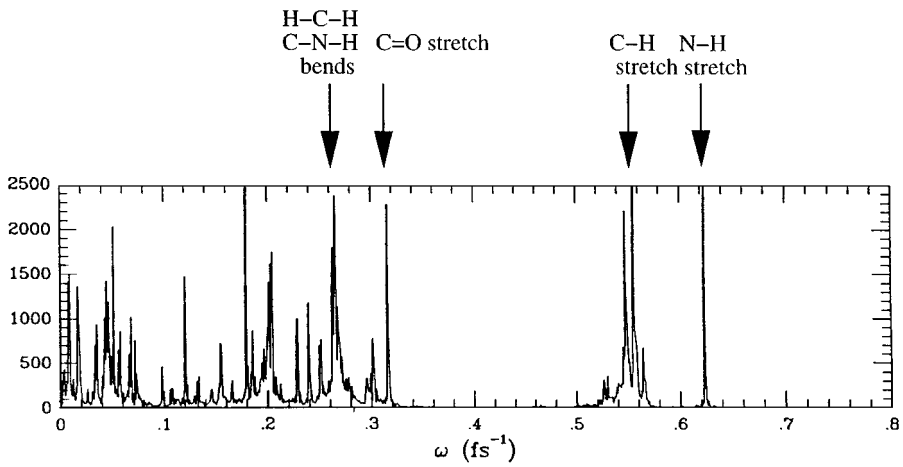

FIG. 9. Power spectrum for the dipeptide from an IM trajectory using $\Delta t = 0.5$ fs, with some typical frequencies identified.

TABLE 2
Timesteps for the 3 : 1 and 4 : 1 Resonances of N–H and C–H Vibrations According to Analysis of One-Dimensional Systems for IM and Verlet Integrators

Resonance order	Verlet		IM	
	N–H	C–H	N–H	C–H
$n = 3$	2.8	3.2	5.5	6.3
$n = 4$	2.2	2.6	3.2	3.6

Note. The estimates for the resonant timesteps from a one-dimensional [14] analysis are obtained as follows. Equation (9) of the text gives the timestep and method-dependent angular frequency for the symplectic method: $\theta_{\text{eff}} = \omega_{\text{eff}} \Delta t = 2 \arcsin(\sqrt{\phi}\omega\Delta t/2)$, where $\phi = (1 + \alpha(\omega\Delta t)^2)^{-1}$ and ω is the natural frequency of the system. For IM $(\alpha = 1/4)$ $\omega_{\text{eff}} = (2/\Delta t) \arctan(\omega\Delta t/2)$, and for Verlet $(\alpha = 0)$ $\omega_{\text{eff}} = (2/\Delta t) \arcsin(\omega\Delta t/2)$. As derived in Ref. [14], the resonant timestep of order $n : m$ can be obtained by using the function ω_{eff} in the expression $n\Delta t\omega_{\text{eff}} = 2\pi m$, since those timesteps correspond to a sampling of n phase-space points in m revolutions. This substitution yields $\Delta t = (2/\omega) \tan(\pi m/n)$ for IM and $\Delta t = (2/\omega) \sin(\pi m/n)$ for Verlet. For $n = 3, 4$, and $m = 1$, we have: $\Delta t_{3,1} = 2\sqrt{3}/\omega$ and $\Delta t_{4,1} = 2/\omega$ for IM; $\Delta t_{3,1} = \sqrt{3}/\omega$ and $\Delta t_{4,1} = \sqrt{2}/\omega$ for Verlet.

for IM, the analysis of N–H and C–H stretching vibrations alone is insufficient to explain the instability onset at about 4.5 fs.

Figure 10 displays the average kinetic (E_{k}) and potential (E_{p}) energy, as well as the E_{p} components, for IM. We see that E_{k} and E_{p} are partitioned nearly equally and reflect the pattern of instabilities of the total energy. Bond-stretching, as well as angle-bending energies increase significantly in the region of instabilities; in contrast, torsional, van der Waals (vdW), and electrostatic contributions remain nearly constant throughout the range of timesteps examined. The rapid growth of the angle-bending energy—as fast as the bond-stretching term—was surprising. This points to a strong coupling between the two modes in the timestep region of instability.

Figure 11 follows the timestep variation of the power spectrum obtained for a hydrogen atom involved in an N–H bond for the IM method. The position of the high frequency peak follows the predicted value according to Eq. (9). Hence, we expect 3 : 1 resonance to occur at $\Delta t = 5.5$ fs. Indeed, the plots in Fig. 12 of the bond length evolution at this timestep for both N–H bonds, as well as for the nearby $\Delta t = 5.2$ and $\Delta t = 5.7$ fs, show three branches. These branches indicate the proximity to third-order resonance. Yet, judging from the rate of average energy growth, the instability at $\Delta t = 5.5$ fs appears weaker than at $\Delta t = 5.2$ or 5.7 fs.

The average values of N–H bond lengths and their fluctuations, although not converged, do not reveal any growth at the timesteps associated with resonance. This suggests that the N–H bond resonance does not cause the instability observed, even though it has the shortest period. To confirm this, we modified the stretching constants for the N–H bond terms by decreasing their value by about 30%. Indeed, this increase in the associated period did not remove instabilities at $\Delta t = 5.2$, 5.5, and 5.7 fs. Clearly, the N–H bond stretch, modeled by a harmonic potential (for which IM is stable) is not the culprit here: the nonlinear forces acting on the bond are not sufficiently strong to induce instability.

What, then, is the origin of this instability? Inspection of the average values of bond lengths and their fluctuations (though not well converged) points to the C–H bonds as a possible source. The variation of the power spectrum with the timestep obtained for one

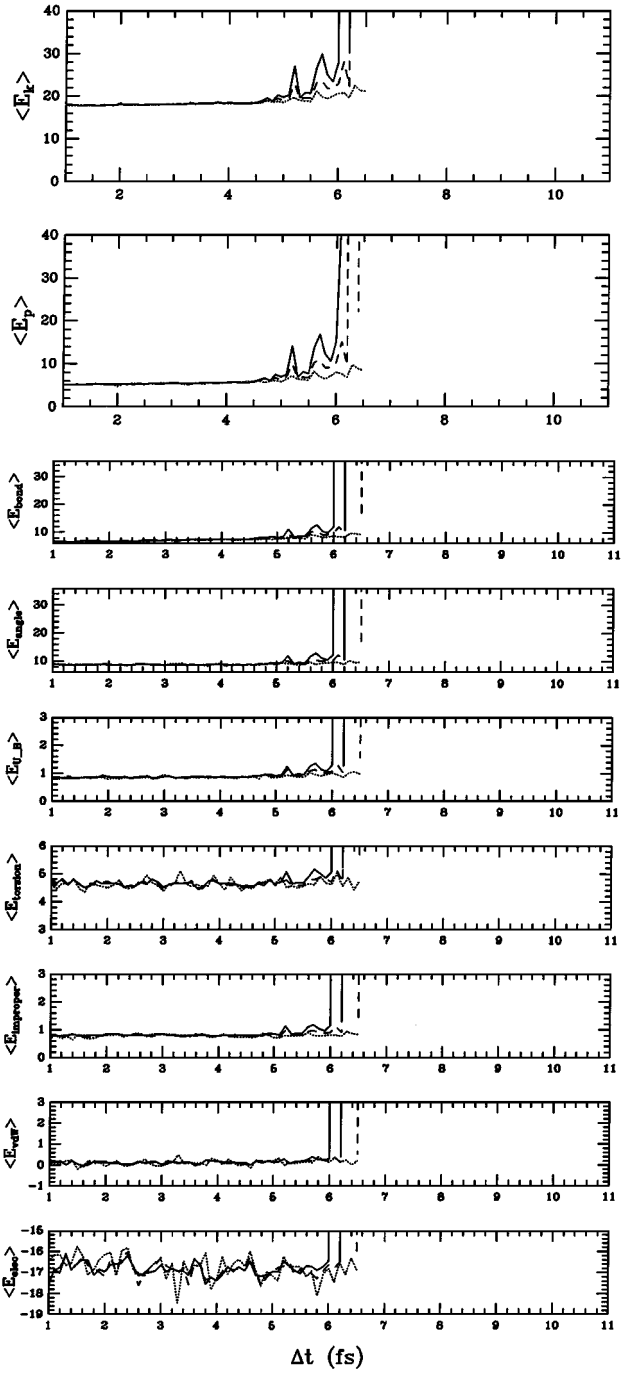

FIG. 10. Average kinetic (E_k) and potential (E_p) energy, as well as E_p components, for the IM scheme for the dipeptide model. The three lines correspond to averaging energies over an increasing number of steps: 2×10^4 (dotted line); 6×10^4 (dashed line); and 10^5 (solid line).

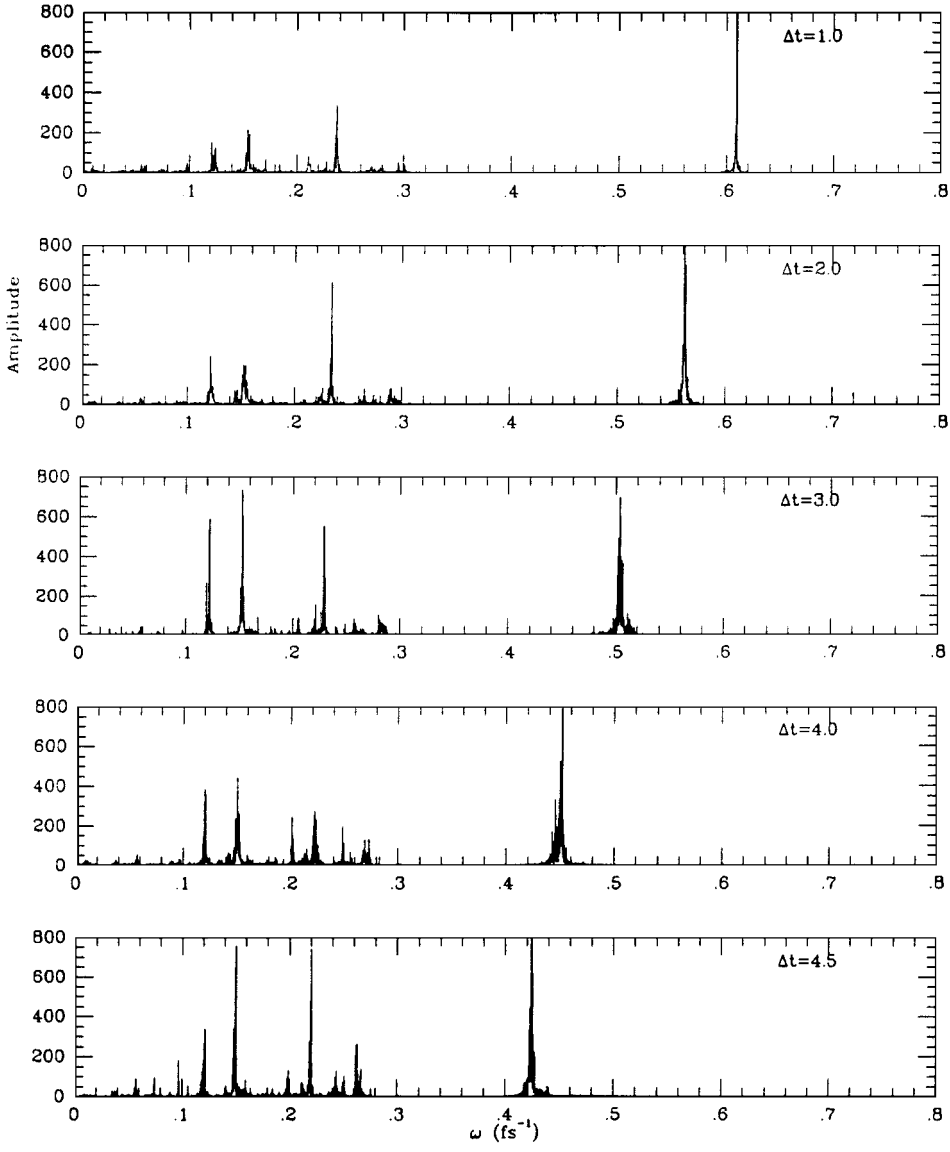

FIG. 11. Timestep variation of the power spectrum for a hydrogen atom in an N–H bond as obtained from the IM trajectory.

C–H bond in a methyl group is presented in Fig. 13. While the main peak follows the expected shift of frequency with the timestep (Eq. (9)), a band of lower amplitude peaks appears on the high-frequency region of the main band for $\Delta t > 2.0$ fs. This band ends with a peak in the region of 0.46–0.50 fs^{-1}, which does not follow the prediction of Eq. (9). This peak is only slightly shifted toward lower values of frequencies with increasing Δt.

The instability caused by this peak should occur just below the 4.5 fs timestep. This band might result from a timestep-corrupted coupling between the C–H bond stretching and H–C–H angle bending modes. This coupling increases in strength due to the timestep-induced shift of frequencies. A large increase of the angle-bending energy in the instability region gives further support to our suggestion that angle bending may be an instability

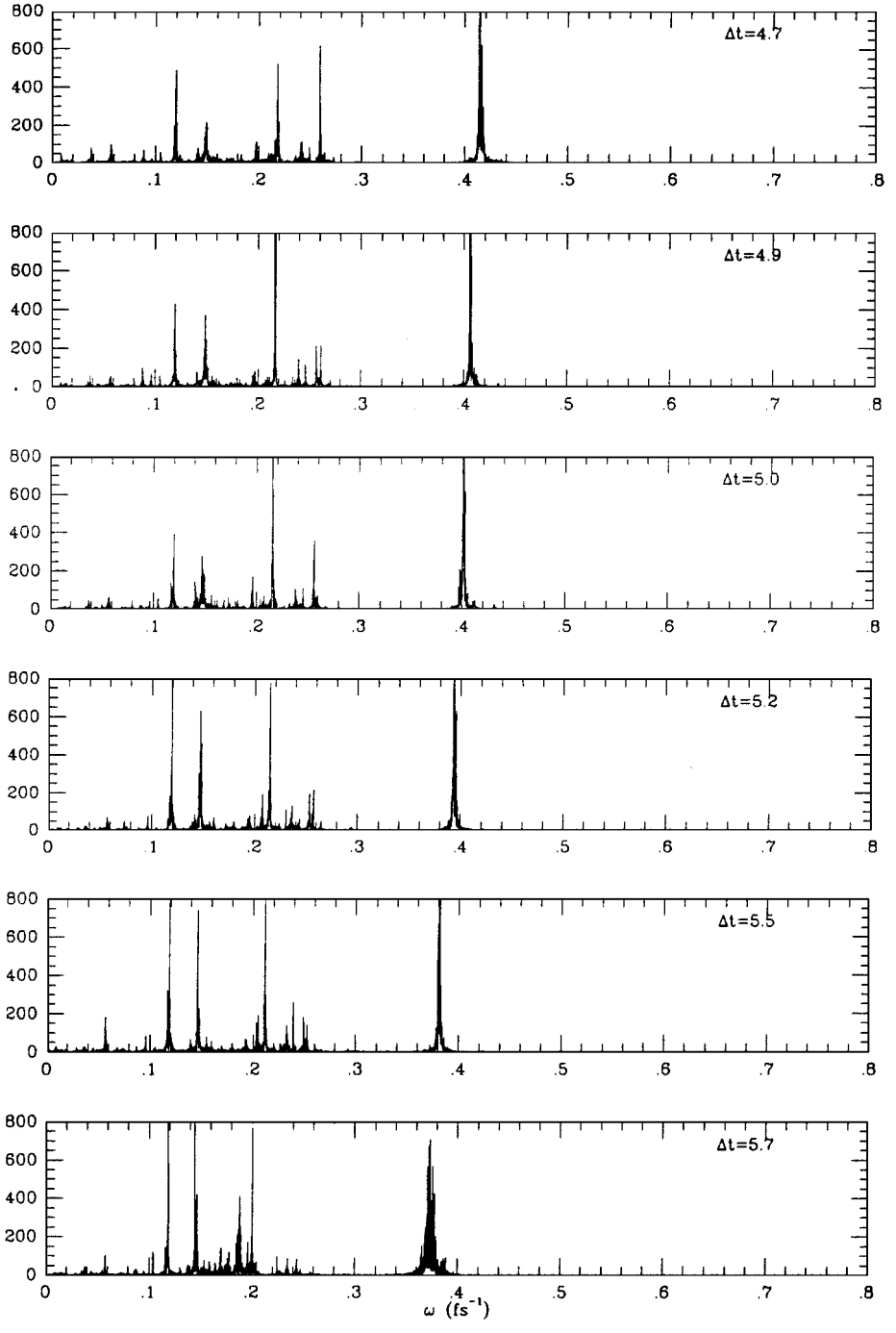

FIG. 11—*Continued*

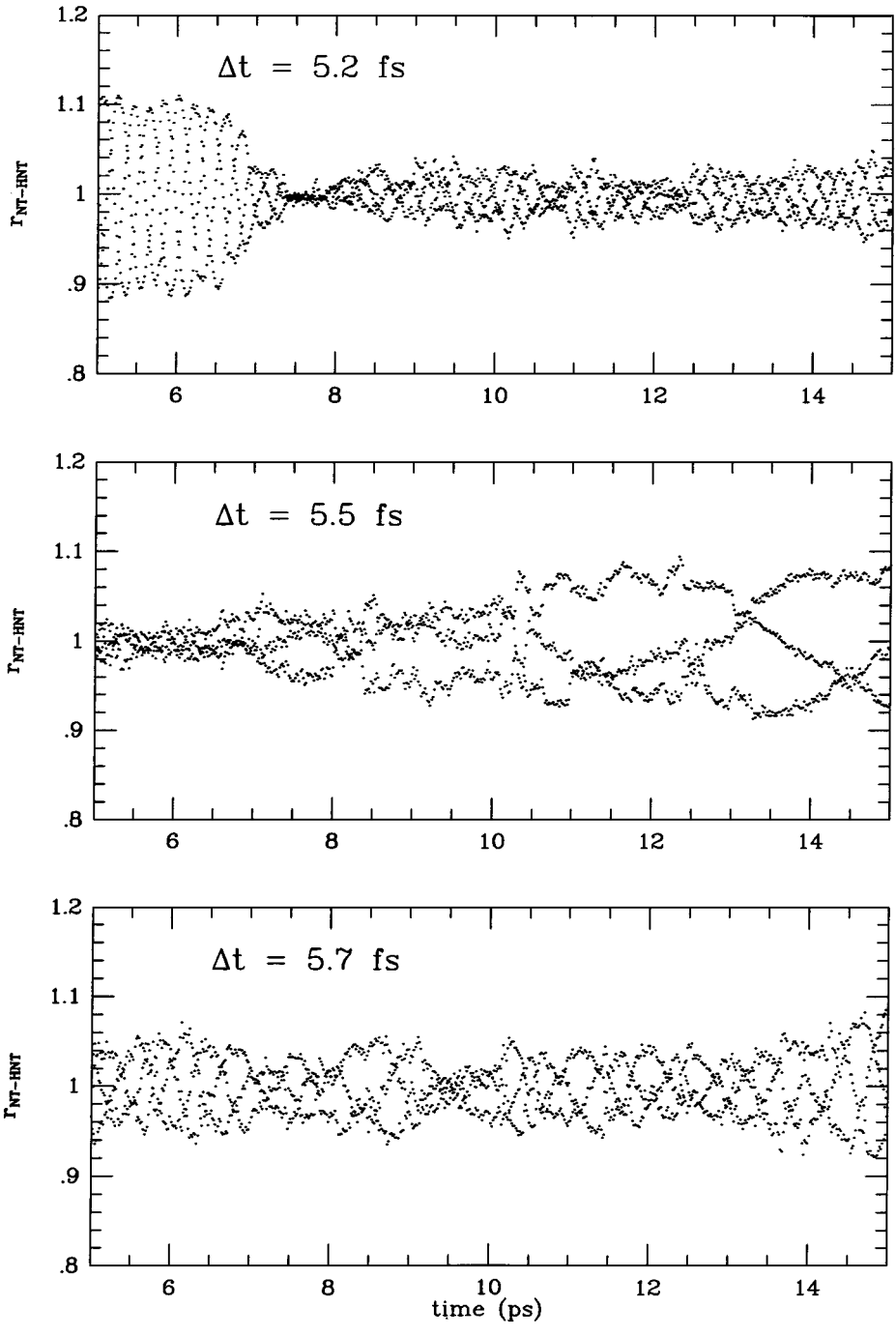

FIG. 12. Bond-length evolution for the dipeptide at timesteps $\Delta t = 5.2$, $\Delta t = 5.5$, and $\Delta t = 5.7$ fs for both N–H bonds, corresponding to the IM trajectory model.

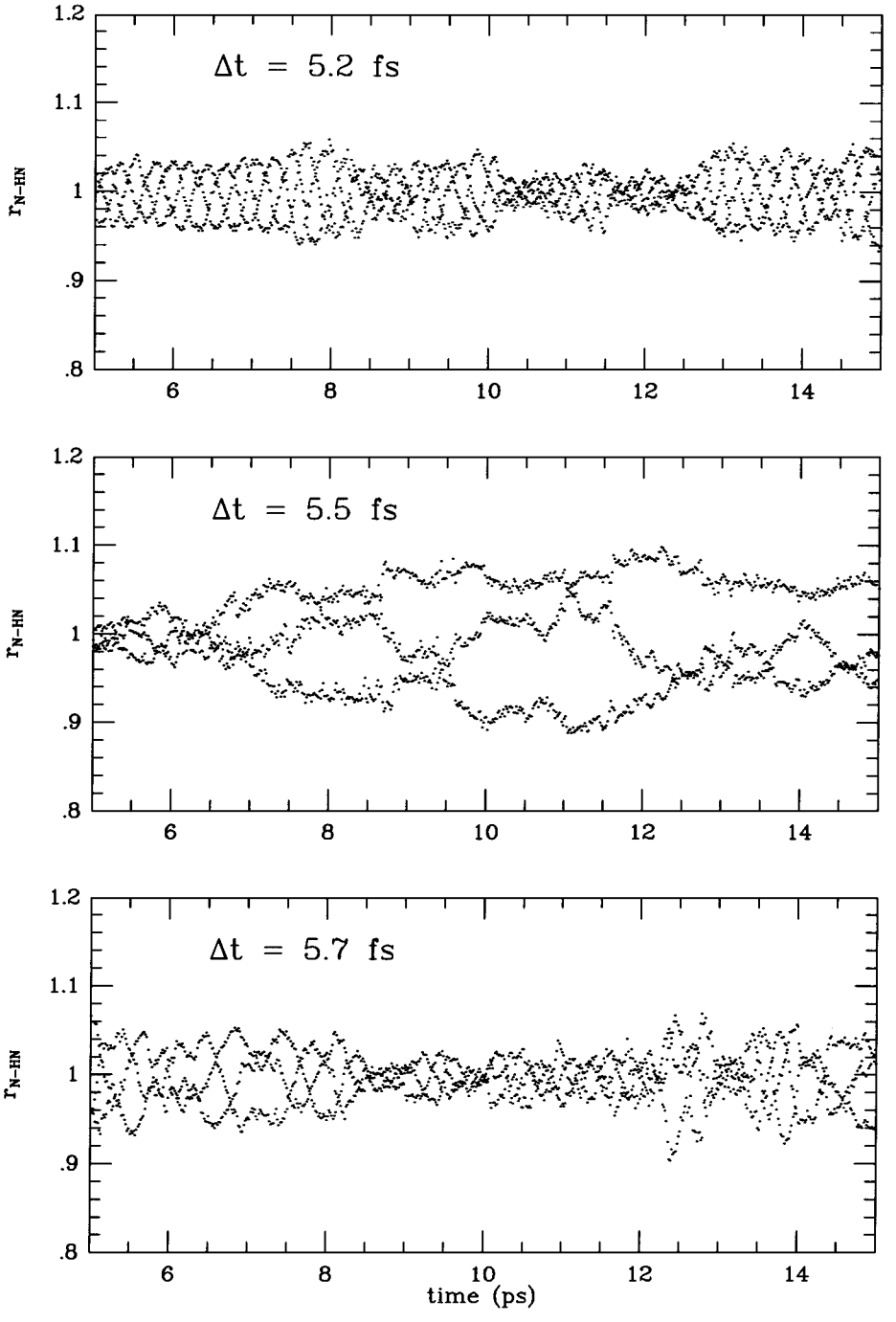

FIG. 12—*Continued*

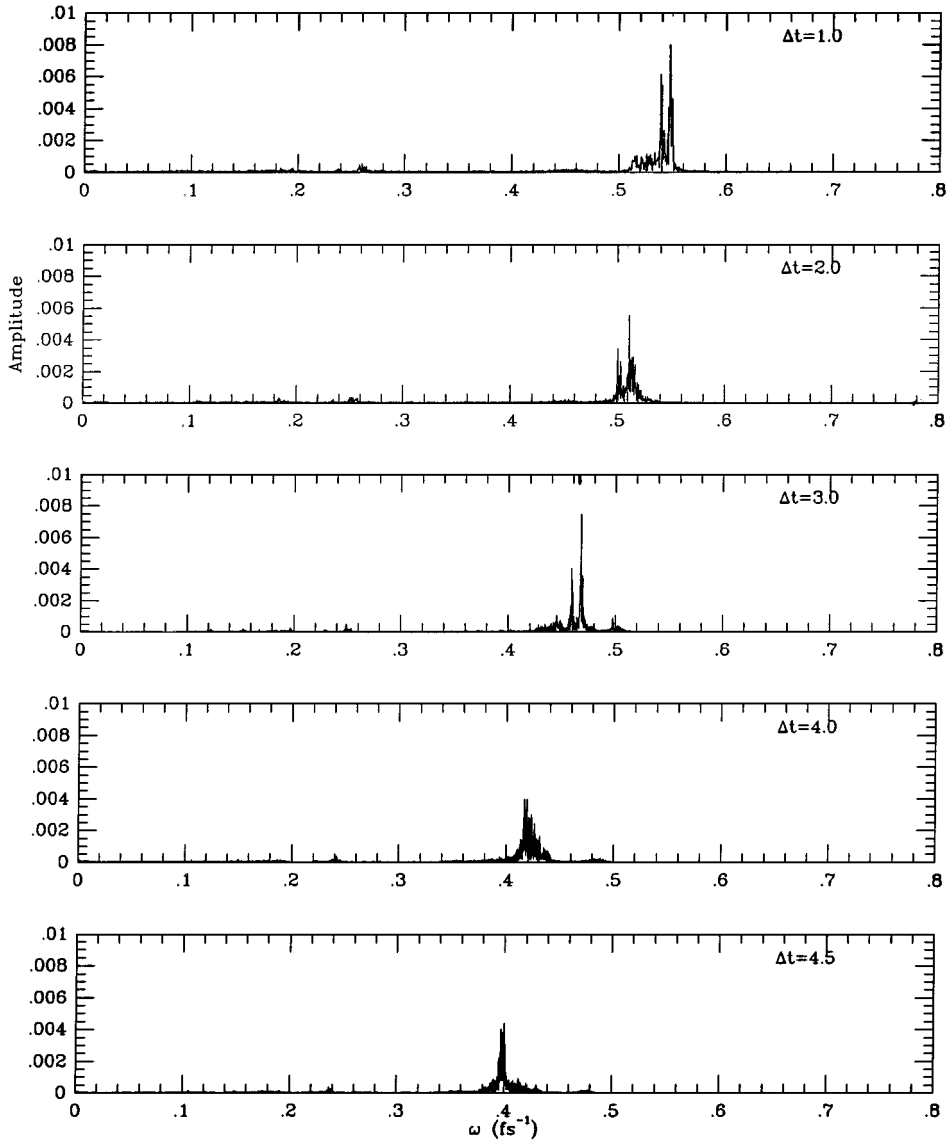

FIG. 13. Variation of the power spectrum with the timestep for one C–H bond in a methyl group for the IM trajectory of alanine dipeptide.

culprit. Inspection of the spectrum for $\Delta t = 5.2$ fs in Fig. 13 shows a small peak around 0.405 fs^{-1}, which may be in resonance of order 3 with Δt. Indeed, a decrease of C–H bond-stretching force constant successfully eliminated instability for $\Delta t = 5.2$ fs (as seen from the 100,000-step simulations). Still, instability remained at $\Delta t = 5.5$ or 5.7 as before.

For $\Delta t = 5.7$ fs and higher, the onset of instability is very fast. There are at least three possible explanations to this observation of chaotic behavior.

First, adequate averaging for the Hamiltonian trajectory cannot occur when the timestep is so large.

Second, instability may be caused by an *overlap* of the principal timestep resonances. Such chaotic zones induced by an overlap of resonances associated with the high-frequency

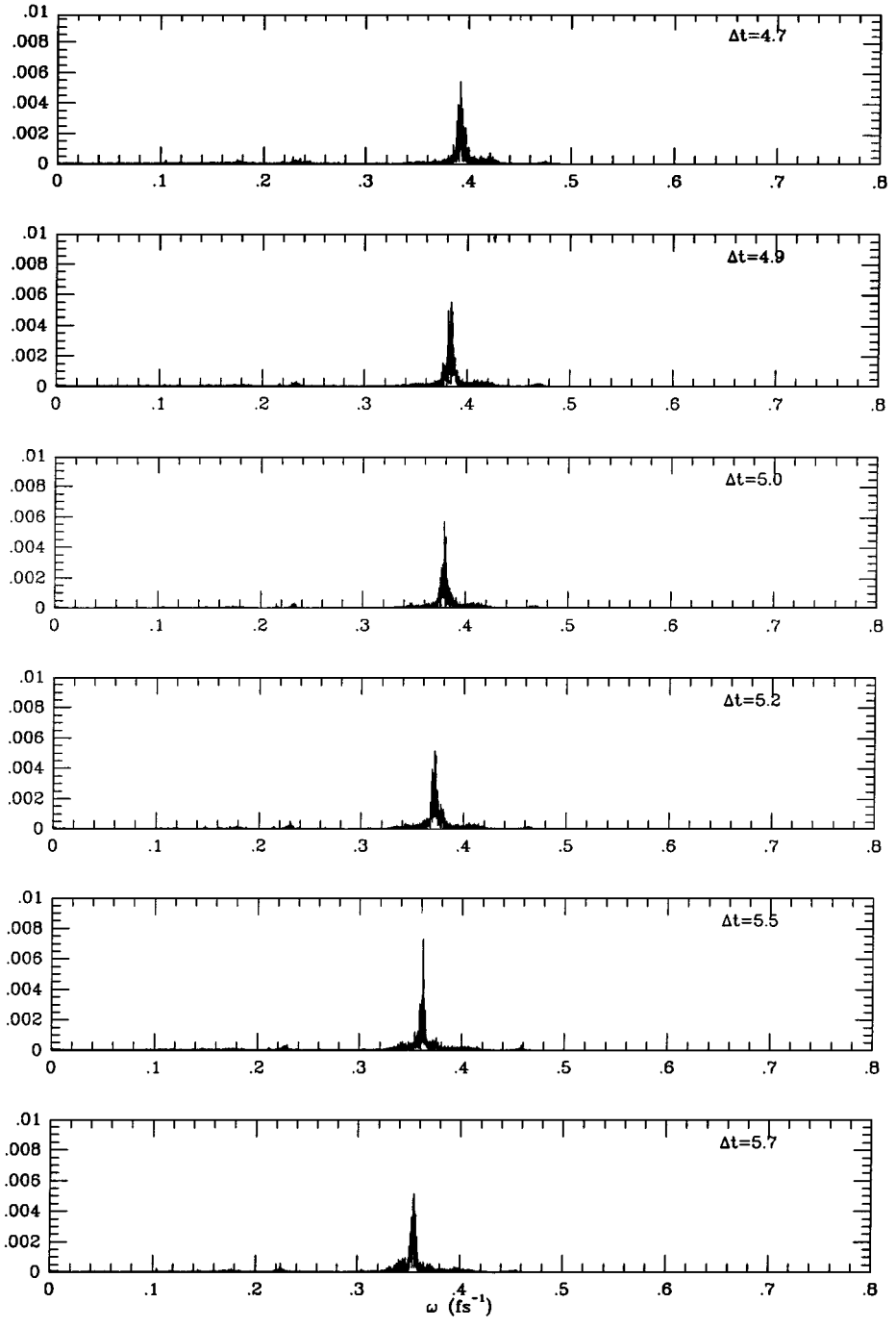

FIG. 13—*Continued*

terms are revealed by Wisdom and Holman through their nonlinear stability analysis of the symplectic mapping for a planetary n-body problem [27]. They determine the borders and mechanisms of these gross instabilities through the application of heuristic tools of nonlinear dynamics such as the Chirikov overlap criterion. Such criteria for estimating the widths of chaotic zones have been associated with regions near the pendulum separatrix; the closer a trajectory is to the separatrix the smaller the timestep must be to avoid this gross instability. This situation might only be relevant to molecular systems when the energy is large, say close to the bond dissociation limit.

A third possibility for the observed instability is some transient, nonlinear, and high-frequency motion present in the system's dynamics. Small, cumulative local fluctuations can induce sudden and large conformational changes, even for a relatively small system such as our dipeptide. Nonbonded interactions are one possible source of instability that limit the timestep in MD simulations. We find that the van der Waals energy does not increase substantially with the timestep (Fig. 10) for the dipeptide, but changes in the electrostatic component are larger. For a molecular system in solvent, both forces are expected to be stronger and play a major role in governing the system's dynamics. In addition, the formation and breakage of inter- and intramolecular hydrogen bonds for a solvated macromolecule can dramatically increase the likelihood of instabilities [21].

6. CONCLUSIONS

This work examined the intriguing phenomenon of resonance in MD simulations. Resonance is a pronounced integrator-induced corruption of a system's dynamics. This source of timestep limitation is not well appreciated, in general, and certainly analyses of resonance patterns have been few in connection to MD. Nonetheless, resonances are present in the commonly used Verlet integrator [15], as well as in symplectic implicit schemes typically associated with favorable properties. These resonances can only be avoided by restricting the timestep beyond estimates based on linear stability. Formulas for this purpose are given in Tables 1 and 2. Table 1, in particular, includes timestep thresholds for the popular Verlet method.

As an extension of our resonance analysis for the implicit midpoint (IM) method [15], we considered here a family of symplectic implicit schemes, parameterized by α, that exhibit different resonance patterns. Our goal was to eliminate the most severe resonances (third and fourth order) observed for IM ($\alpha = \frac{1}{4}$) that lead to instability and very large energies, respectively, on a Morse oscillator. Our theory suggested that both the EW ($\alpha = \frac{1}{3}$) and LIM2 ($\alpha = \frac{1}{2}$) integrators are better than IM since the limit on the maximum possible phase-angle-change per timestep is smaller than IM (Fig. 1). Thus, according to linear stability analysis, the EW method eliminates the third-order resonance, and LIM2 eliminates both third- and fourth-order resonances.

Our numerical experiments on two simple nonlinear systems—a Morse oscillator and a Lennard–Jones system—confirmed this analysis. That is, methods can be designed to remove specific resonances. Furthermore, our application to a more complex dipeptide model found EW and LIM2 to yield improvements over IM when the timestep was large relative to the fastest frequency of the system. Still, the growth of energy fluctuations with the timestep, although far less erratic than that of IM, is large for EW and LIM2 when $\Delta t > 6$ fs. For small timesteps, the increase of the systematic discretization error with the

timestep is 3 and 5 times larger than Verlet, respectively, for EW and LIM2. Together with the added cost of the implicit formulation (minimization of a nonlinear function at each timestep), the benefits of using these schemes is unclear, even if high accuracy is not commensurate with the accuracy of the governing force fields. One possible utility of the methods developed here at such large timestep regimes is for enhanced sampling purposes. Such sampling questions may be overall more important in macromolecular simulations than determining a system's dynamics.

Interesting also for the dipeptide was our analysis of the resonance patterns of IM. We found linear analysis to be helpful but not sufficient for identifying the timesteps at which resonance should occur (fractions of the characteristic period). In particular, it was difficult to attribute resonance to one particular vibrational mode. Rather, we found that the complex interplay among intramolecular modes—namely bond stretching, angle bending, and torsional motion—leads to instabilities at much shorter timesteps than dictated by linear analysis. This is true for all the implicit methods analyzed here (which are A-stable). Hence, the notion of resonance is blurred for multiple-timescale systems.

The tools presented here—a family of implicit symplectic integrators, postprocessing, and predictive resonance theory for nonlinear systems—might also be useful in general for analyzing biomolecular dynamics. Clearly, our EW and LIM2 methods are steps in the right direction to eliminate nonlinear resonance—since they are effective on simple systems. However, the nonlinear scaling of frequencies with the timestep poses a problem for multidimensional systems, and further enhancements in this class of symplectic implicit methods are required if much larger timesteps will be used.

An important related problem is the noted resonance [3, 4, 8, 12] exhibited by symplectic generalizations of the Verlet method to multiple timesteps [10, 26]. These methods use a large timestep for the slowly varying forces and are most likely limited to 4 or 5 fs, near half the period of the fastest motion. The resonances observed for multiple-timestep schemes occur for linear as well as nonlinear problems [8] and thus differ from the type of resonance discussed in this article. A linear analysis for several multiple-timestep schemes in Barth and Schlick [3] shows that resonance can be eliminated by a special merging of the slow and fast forces, as used in the LN (so called for its origin in a Langevin/Normal-mode) scheme [2]. The successful idea used in LN can be generally applied. A symplectic scheme for overcoming the 5-fs timestep barrier has also been proposed [8].

ACKNOWLEDGMENTS

We are grateful to Vera Koffman for producing Figs. 1 and 6, to Yong Wen for Figs. 2, 3, and 4, and to John Lin for Fig. 5. We also thank John Johnson for technical assistance. The work of T. Schlick and M. Mandziuk is supported by the National Institutes of Health (Research Resources RR08102), the National Science Foundation (PYI Award ASC-9157582) and the Alfred P. Sloan Foundation. The work of R. D. Skeel was performed in part while visiting the Courant Institute and was supported by NSF Grant DMS-9600088, by NIH Grant P41RR05969, and by NSF Grant BIR-9318159. T.S. is an investigator for the Howard Hughes Medical Institute.

REFERENCES

1. V. I. Arnold, *Mathematical Methods of Classical Mechanics* (Springer-Verlag, New York, 1989).
2. E. Barth, M. Mandziuk, and T. Schlick, A separating framework for increasing the timestep in molecular dynamics, in *Computer Simulation of Biomolecular Systems: Theoretical and Experimental Applications*,

edited by W. F. van Gunsteren, P. K. Weiner, and A. J. Wilkinson, Vol. 3, p. 97 (Chap. 4) (ESCOM, Leiden, The Netherlands, 1997).

3. E. Barth and T. Schlick, Overcoming stability limitations in biomolecular dynamics: Combining force splitting via extrapolation with Langevin dynamics in LN, preprint, 1997.
4. T. Bishop, R. D. Skeel, and K. Schulten, Difficulties with multiple timestepping and the fast multipole algorithm in molecular dynamics, *J. Comput. Chem.* **18**(14), 1785 (1997).
5. B. R. Brooks, R. E. Bruccoleri, B. D. Olafson, D. J. States, S. Swaminathan, and M. Karplus, CHARMM: A program for macromolecular energy, minimization, and dynamics calculations, *J. Comput. Chem.* **4**(2), 187 (1983).
6. P. Derreumaux and T. Schlick, Long-time integration for peptides by the dynamics driver approach, *Proteins: Struc. Func. Gen.* **21**, 282 (1995).
7. R. Elber, Novel methods for molecular dynamics simulations, *Curr. Opin. Struc. Biol.* **6**, 232 (1996).
8. B. García-Archilla, J. M. Sanz-Serna, and R. D. Skeel, Long-time-step methods for oscillatory differential equations, *SIAM J. Sci. Comput.*, to appear. [Tech. Rep. 1996/7, Dept. Math. Aplic. Comput., Univ. Valladolid, Valladolid, Spain]
9. O. Gonzalez and J. Simo, On the stability of symplectic and energy-momentum algorithms for nonlinear Hamiltonian systems with symmetry, *Comput. Methods Appl. Mech. Eng.* **134**, 197 (1996).
10. H. Grubmüller, H. Heller, A. Windemuth, and K. Schulten, Generalized Verlet algorithm for efficient molecular dynamics simulations with long-range interactions, *Molecular Simulation* **6**, 121 (1991).
11. M. H. Hao, M. R. Pincus, S. Rackovsky, and H. A. Scheraga, Unfolding and refolding of the native structure of bovine pancreatic trypsin inhibitor studied by computer simulations, *Biochemistry* **32**, 9614 (1993).
12. D. Janežič and F. Merzel, An efficient symplectic integration algorithm for molecular dynamics simulations, *J. Chem. Inf. Comput. Sci*. **35**, 321 (1995).
13. B. J. Leimkuhler, S. Reich, and R. D. Skeel, Integration methods for molecular dynamics, in *Mathematical Approaches to Biomolecular Structure and Dynamics*, edited by J. P. Mesirov, K. Schulten, and D. W. Sumners, Vol. 82 of *IMA Volumes in Mathematics and its Applications*, p. 161 (Springer-Verlag, 1996).
14. M. López-Marcos, J. M. Sanz-Serna, and R. D. Skeel, Cheap enhancement of symplectic integrators, in *Numerical Analysis 1995*, edited by D. F. Griffiths and G. A. Watson, p. 107 (Longman Group, London, 1996).
15. M. Mandziuk and T. Schlick, Resonance in the dynamics of chemical systems simulated by the implicit midpoint scheme, *Chem. Phys. Letters* **237**, 525 (1995).
16. R. I. McLachlan and P. Atela, The accuracy of symplectic integrators, *Nonlinearity* **5**, 541 (1992).
17. C. S. Peskin and T. Schlick, Molecular dynamics by the backward Euler method, *Comm. Pure and Appl. Math.* **42**, 1001 (1989).
18. A. Rahman, Correlation in the motion of atoms in liquid argon, *Phys. Rev. A* **136**, 405 (1964).
19. J. Sanz-Serna and M. Calvo, *Numerical Hamiltonian Problems* (Chapman & Hall, London, 1994).
20. J. M. Sanz-Serna, Two topics in nonlinear stability, in *Advances in Numerical Analysis*, edited by W. Light, (Clarendon Press, Oxford, 1991).
21. T. Schlick, E. Barth, and M. Mandziuk, Biomolecular dynamics at long timesteps: Bridging the timescale gap between simulation and experimentation, *Ann. Rev. Biophys. Biomol. Struc.* **26**, 179 (1997).
22. T. Schlick and A. Fogelson, TNPACK—A truncated Newton minimization package for large-scale problems. I. Algorithm and usage, *ACM Trans. Math. Software* **18**(46), 46 (1992).
23. J. C. Simo and N. Tarnow, The discrete energy-momentum method. Conserving algorithms for nonlinear elastodynamics, *ZAMP* **43**, 757 (1992).
24. J. C. Simo and N. Tarnow, *A Review of Conserving Algorithms for Nonlinear Dynamics*, Technical Report SUDAM Report 92-7, Department Mechanical Engineering, Stanford University, 1992.
25. R. D. Skeel, G. Zhang, and T. Schlick, A family of symplectic integrators: Stability, accuracy, and molecular dynamics applications, *SIAM J. Sci. Comput.* **18**(1), 203 (1997).
26. M. Tuckerman, B. J. Berne, and G. J. Martyna, Reversible multiple time scale molecular dynamics, *J. Chem. Phys.* **97**(3), 1990 (1992).

27. J. Wisdom and M. Holman, Symplectic maps for the n-body problem: Stability analysis, *Astr. J.* **104**(5), 2022 (1992).
28. G. Zhang and T. Schlick, LIN: A new algorithm to simulate the dynamics of biomolecules by combining implicit-integration and normal mode techniques, *J. Comput. Chem.* **14**, 1212 (1993).
29. G. Zhang and T. Schlick, Implicit discretization schemes for Langevin dynamics, *Mol. Phys.* **84**, 1077 (1995).
30. M. Zhang and R. D. Skeel, Cheap implicit symplectic integrators, *Appl. Num. Math.* **25** (1997).